Research Article

INTERNATIONAL JOURNAL OF ADVANCED ROBOTIC SYSTEMS

International Journal of Advanced Robotic Systems
January-February 2020: 1–11

DOI: 10.1177/1729881419894417
journals.sagepub.com/home/arx
SAGE

A model-free fuzzy adaptive trajectory tracking control algorithm based on dynamic surface control

Mingsi Tong[1,2], Weiyang Lin[1,2], Xiang Huo[2], Zishu Jin[2] and Chengzong Miao[2]

Abstract

According to the robot's dynamics, a high performance algorithm based on dynamic surface control is introduced to track desired trajectory, and simulations are conducted on a selective compliance assembly robot arm-type manipulator to verify the algorithm. The traditional dynamic surface control is designed based on dynamic model, which requires exact model information. Due to the model uncertainty and complex environments, the tracking performance of the controller can be significantly decreased. Therefore, a model-free fuzzy adaptive dynamic surface controller is designed, by adopting a fuzzy system with Lyapunov self-adaptation law. The new controller efficiently improves the dynamic quality. The simulation results prove that the designed model-free controller ensures that all the states and signals of the closed-loop system are bounded, the system has a faster response speed and smaller steady-state error comparing with the traditional dynamic surface control using the selective compliance assembly robot arm model, and the tracking error converge to a very small scale. Besides, the proposed algorithm can track the desired trajectory with high performance without the prior knowledge of specific parameters from the experimental manipulator, which simplifies the complexity of building the control system.

Keywords

Trajectory tracking, dynamic surface control, fuzzy control, adaptive control

Date received: 16 April 2019; accepted: 17 November 2019

Topic: Robot Manipulation and Control
Topic Editor: Andrey V Savkin
Associate Editor: Bin He

Introduction

Robot trajectory tracking has wide applications in robotic systems. Robotic motion control problems with constraints require novel control laws to improve the performance.[1–3] Given the track profile function, Abad et al.[4] designed an optimal navigation algorithm for unmanned ground vehicle; Coelho and Nunes[5] implemented a Kalman-based active observer controller under nonholonomic constraints on wheeled mobile robots, to improve the robustness of the path following; and Matveev et al.[6] proposed a sliding mode strategy which can be used for the navigation of a unicycle-like robot under moving obstacles.

Since the first selective compliance assembly robot arm (SCARA) was designed by Hiroshi Makino in 1978, this kind of four-degree robot is widely used in industries, high-speed and precision of motion.[7] Such as handling, assembly, welding and other applications. Because

[1] Key Laboratory of Micro-systems and Micro-structures Manufacturing of Ministry of Education, Harbin Institute of Technology, Harbin, China
[2] Research Institute of Intelligent Control and Systems, Harbin Institute of Technology, Harbin, China

Corresponding author:
Weiyang Lin, Key Laboratory of Micro-systems and Micro-structures Manufacturing of Ministry of Education, Harbin Institute of Technology, Harbin 150001, China; Research Institute of Intelligent Control and Systems, Harbin Institute of Technology, Harbin 150001, China.
Email: wylin@hit.edu.cn

SCARA's control model is highly non-linear, time-varying, and strongly coupled, and it is prone to vibration and shock during operation, which makes the high-performance control of SCARA very difficult, so it needs to design advanced control algorithms for it.[8,9]

Backstepping control had long been a powerful tool for dealing with nonlinear systems with parametric uncertainties. However, there is a problem of "explosion of terms"[10] in the backstepping design algorithm, which greatly increases the amount of computation. To solve this problem, Swaroop et al. proposed the dynamic surface control (DSC) algorithm[11] by introducing a low-pass filter into the backstepping design process. Then a series of controllers for nonlinear systems were proposed, based on DSC.[12–16]

Although the DSC algorithm solves the problem of the dimension explosion of backstepping, the DSC control law based on the dynamic model needs to control the dynamic parameters of the target, which weakens the anti-interference ability of the closed-loop system. Adaptive fuzzy controller has been researched by many scholars, and it can be used to decrease the negative influence caused by robot model uncertainty. For example, Soltanpour et al.[17] used adaptive fuzzy sliding mode control to approximate nonlinear and uncertain robot dynamics. Long et al.[18] built an adaptive neural network control method to realize high-precision manipulator position tracking. Chen[19] achieved a dynamic fuzzy network to solve the *n*-link robot manipulator tracking control problems.

To realize a control law without model parameters and improve the tracking speed, DSC algorithm combined with adaptive controller and fuzzy state observer is proposed in paper.[20–22] However, many research studies lack the industrial scene application. The proposed DSC algorithm which achieves a whole closed-loop system not only satisfies the desired dynamic and static performance but also guarantees a high performance tracking trajectory.[23] Fuzzy logic systems are used to approach the uncertain model functions of the control target.[24] The proposed algorithm guarantees the uniform boundedness of all the signals in the closed-loop system. By choosing the appropriate controller parameters, the tracking error can be significantly restrained[25]; this method can significantly decrease the external disturbance and internal uncertainty caused by the robot model.

SCARA-type manipulator

SCARA-type robots are characterized by its small load and fast speed. They are mainly used in such applications as fast sorting, precision assembly in computing, communication, and consumer (3C) industry, food industry, and so on. Thus, this kind of robot is used for analyzing in this article, due to the unique structure and its wide usage.[26,27]

Kinematic analysis of SCARA

The kinematics of SCARA robot is considered first, which is an important basis for studying robot dynamics and control.

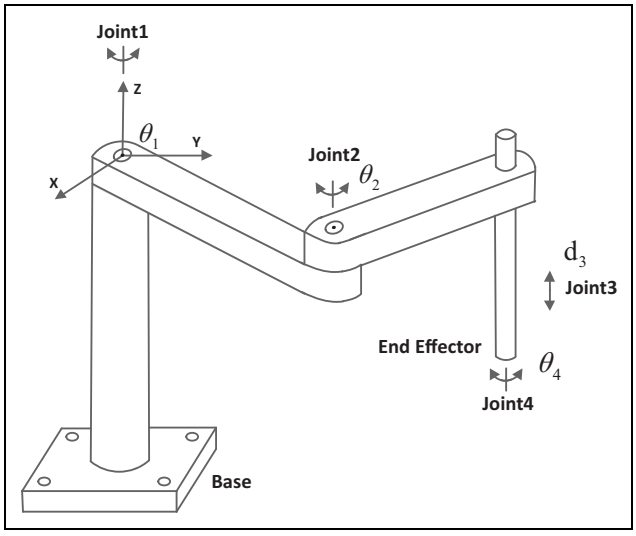

Figure 1. A typical SCARA structure with four joints. SCARA: selective compliance assembly robot arm.

Table 1. The DH parameter assignment of the SCARA.

Joint *i*	α_i	a_i	d_i	θ_i
1	0	0	d_1	θ_1
2	0	1	0	θ_2
3	180°	1	d_3	0
4	0	0	0	θ_3

SCARA: selective compliance assembly robot arm.

Figure 1 shows an abstract SCARA structure and the base coordinate of the position and attitude. The Denavit–Hartenberg (DH) parameter[28] of the SCARA is given in Table 1.

Applying the homogeneous transformations given by

$$ {}^{i-1}\mathbf{T}_i = \begin{bmatrix} \mathrm{c}\theta_i & -\mathrm{s}\theta_i & 0 & a_i \\ \mathrm{s}\theta_i \mathrm{c}\alpha_i & \mathrm{c}\theta_i \mathrm{c}\alpha_i & -\mathrm{s}\alpha_i & -d_i \mathrm{s}\alpha_i \\ \mathrm{s}\theta_i \mathrm{s}\alpha_i & \mathrm{c}\theta_i \mathrm{s}\alpha_i & \mathrm{c}\alpha_i & d_i \mathrm{c}\alpha_i \\ 0 & 0 & 0 & 1 \end{bmatrix} \quad (1) $$

where $\mathrm{s}\theta_i$, $\mathrm{c}\theta_i$, $\mathrm{s}\alpha_i$, and $\mathrm{c}\alpha_i$ represent $\sin\theta_i$, $\cos\theta_i$, $\sin\alpha_i$, and $\cos\alpha_i$, respectively. Then the direct kinematic model can be expressed with

$$ \mathbf{T} = \begin{bmatrix} T_{11} & T_{12} & 0 & T_{14} \\ T_{21} & T_{22} & 0 & T_{24} \\ 0 & 0 & -1 & d_1 - d_3 \\ 0 & 0 & 0 & 1 \end{bmatrix} \quad (2) $$

where $T_{11} = \cos(\theta_1 + \theta_2 - \theta_4)$, $T_{12} = \sin(\theta_1 + \theta_2 - \theta_4)$, $T_{14} = l_2\cos(\theta_1 + \theta_2) + l_1\cos\theta_1$, $T_{21} = \sin(\theta_1 + \theta_2 - \theta_4)$, $T_{22} = -\cos(\theta_1 + \theta_2 - \theta_4)$, and $T_{24} = l_2\sin(\theta_1 + \theta_2) + l_1\sin\theta_1$.

By using the inverse matrix, each variable in matrix (2) can be recursively introduced. In this article, Euler transformation is introduced to solve the inverse kinematics problem. **T** is the position vector matrix of the end gripper

in the base frame. According to the Euler transformation formula presented with the following equations (3) to (5), it is easy to find the inverse solution of each joint, which is shown in equations (6), (7), (8), and (9), respectively

$$\mathbf{T} = \begin{bmatrix} n_x & o_x & a_x & p_x \\ n_y & o_y & a_y & p_y \\ n_z & o_z & a_z & p_z \\ 0 & 0 & 0 & 1 \end{bmatrix} \tag{3}$$

$$\text{Euler}(\phi, \theta, \psi) = \mathbf{T} \tag{4}$$

$$\text{Euler}(\phi, \theta, \psi) = \text{Rot}(z, \phi)\text{Rot}(y, \theta)\text{Rot}(x, \psi) \tag{5}$$

$$\theta_1 = \text{arctg}\left(\frac{A}{\pm\sqrt{1-A^2}}\right) - \varphi \tag{6}$$

$$\theta_2 = \text{arctg}\left(\frac{r\cos(\theta_1+\varphi)}{r\sin(\theta_1+\varphi) - l_1}\right) \tag{7}$$

$$d_3 = d_1 - p_z \tag{8}$$

$$\theta_4 = \text{arctg}\left(\frac{-n_x\sin\theta_1 + n_y\cos\theta_1}{n_x\cos\theta_1 + n_y\sin\theta_1}\right) - \theta_2 \tag{9}$$

where $A = \frac{p_x^2+p_y^2+l_1^2-l_2^2}{2l_1\sqrt{p_x^2+p_y^2}}$, $\phi = \text{arctg}\frac{p_x}{p_y}$, and $r = \sqrt{p_x^2+p_y^2}$.

Dynamic analysis of SCARA

The dynamic analysis is implemented by employing the Lagrange–Euler formulation which is based on the principle of energy conservation.[29,30] According to the general formula of robot dynamics, the dynamic equations of SCARA robot are established as

$$\boldsymbol{\tau} = \mathbf{M}(\mathbf{q})\ddot{\mathbf{q}} + \mathbf{C}(\mathbf{q}, \dot{\mathbf{q}})\dot{\mathbf{q}} + \mathbf{G}(\mathbf{q}) \tag{10}$$

$$\tau_i = \sum_{j=1}^{n} H_{ij}\ddot{q}_j + \sum_{j=1}^{n}\sum_{k=1}^{n} c_{ijk}\dot{q}_j\dot{q}_k + g_i \tag{11}$$

The gravity expression is

$$\mathbf{G}^{\mathrm{T}} = [0, 0, -(m_3+m_4)g, 0]$$

The moment of inertia, inertia cross product, and first moment of each joint are as

$$I_{1xx} = 0$$

$$I_{1yy} = I_{1zz} = \int_0^{l_1} x^2 dm = \int_0^{l_1} \frac{m_1}{l_1} x^2 dx = \frac{1}{3}m_1 l_1^2$$

$$I_{2xx} = 0, I_{2yy} = I_{2zz} = \frac{1}{3}m_2 l_2^2$$

$$I_{4xx} = I_{4yy} = \frac{1}{3}m_4 l_4^2, I_{4zz} = \frac{1}{2}m_4 R^2$$

$$I_{ixy} = I_{ixz} = I_{iyz} = 0$$

$$m_2\bar{x}_2 = -\frac{1}{2}m_2 l_2, m_2\bar{y}_2 = m_2\bar{z}_2 = 0$$

$$m_3\bar{x}_3 = m_3\bar{y}_3 = 0, m_3\bar{z}_3 = -\frac{1}{2}m_3 l_3$$

$$m_4\bar{x}_4 = m_4\bar{y}_4 = 0, m_4\bar{z}_4 = -\frac{1}{2}m_4 l_4$$

where m_i is the connecting rod quality, l_i is the connecting rod length, and R is the radius of the rolling guide.

The pseudo-inertia matrix of each joint can be obtained according to

$$\mathbf{I}_i = \begin{bmatrix} -I_{11} & I_{ixy} & I_{ixz} & m_i r_{ix} \\ I_{ixy} & I_{22} & I_{iyz} & m_i r_{iy} \\ I_{ixz} & I_{iyz} & I_{33} & m_i r_{iz} \\ m_i r_{ix} & m_i r_{iy} & m_i r_{iz} & m_i \end{bmatrix} \tag{12}$$

where I_{11} is in the form of $\frac{I_{ixx}-I_{iyy}-I_{izz}}{2}$, I_{22} is in the form of $\frac{I_{ixx}-I_{iyy}+I_{izz}}{2}$, and I_{33} is in the form of $\frac{I_{ixx}+I_{iyy}-I_{izz}}{2}$. The positions of the center of gravity for each link are expressed as follows

$$\bar{\mathbf{r}}_1 = \left[-\frac{1}{2}l_1, 0, 0, 1\right]^{\mathrm{T}}, \bar{\mathbf{r}}_2 = \left[-\frac{1}{2}l_2, 0, 0, 1\right]^{\mathrm{T}}$$

$$\bar{\mathbf{r}}_3 = \left[0, 0, -\frac{1}{2}l_3, 1\right]^{\mathrm{T}}, \bar{\mathbf{r}}_4 = \left[0, 0, -\frac{1}{2}l_4, 1\right]^{\mathrm{T}}$$

Combining the above equations, the dynamic model of SCARA is obtained

$$\begin{bmatrix} \tau_1 \\ \tau_2 \\ \tau_3 \\ \tau_4 \end{bmatrix} = \begin{bmatrix} H_{11} & H_{12} & 0 & H_{14} \\ H_{21} & H_{22} & 0 & H_{24} \\ 0 & 0 & H_{33} & 0 \\ H_{41} & H_{42} & 0 & H_{44} \end{bmatrix} \begin{bmatrix} \ddot{q}_1 \\ \ddot{q}_2 \\ \ddot{q}_3 \\ \ddot{q}_4 \end{bmatrix} + \begin{bmatrix} G_1 \\ G_2 \\ G_3 \\ 0 \end{bmatrix} \tag{13}$$

where

$$H_{11} = \frac{1}{3}m_1 l_1^2 + m_2\left(\frac{1}{3}l_1^2 + l_2^2 + l_1 l_2\cos\theta_2\right) + (m_3+m_4)(l_1^2 + l_2^2 + 2l_1 l_2\cos\theta_2) + \frac{1}{4}m_4 R^2$$

$$H_{12} = H_{21} = \frac{1}{3}m_2 l_2^2 + \frac{1}{2}m_2 l_1 l_2\cos\theta_2 + m_3 l_2^2 + m_3 l_1 l_2\cos\theta_2 + m_4 l_2^2 + m_4 l_1 l_2\cos\theta_2 + \frac{1}{2}m_4 R^2$$

$$H_{14} = H_{41} = H_{24} = H_{42} = -\frac{1}{2}m_4 R^2$$

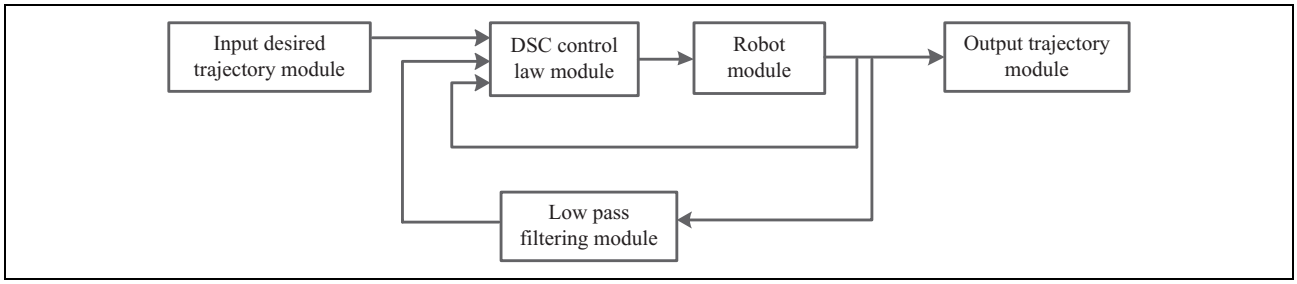

Figure 2. DSC robot system. DSC: dynamic surface control.

$$H_{22} = \frac{1}{3}m_2 l_2 + m_3 l_2^2 + m_4 l_2^2 + \frac{1}{2}m_4 R^2$$

$$H_{33} = m_3 + m_4, H_{44} = \frac{1}{2}m_4 R^2$$

$$G_1 = 2c_{112}\dot{q}_1\dot{q}_2 + c_{122}\dot{q}_2^2$$
$$G_2 = c_{211}\dot{q}_1^2$$
$$G_3 = -(m_3 + m_4)g$$

Dynamic surface control

As mentioned before, the traditional DSC uses dynamic filters to overcome the "explosion of terms." In this section, systematic steps are given to establish DSC, which is employed on the dynamic model of SCARA. The control structure consists of five modules: the input and output trajectory module, the DSC control law module, the robot module, and the low-pass filtering module. The robot control structure is shown in Figure 2.

The robot module contains the parameter information and the dynamic model of the manipulator. According to the dynamic model of SCARA in equation (10), the dynamic character of SCARA can be sorted into

$$\boldsymbol{\tau} = \mathbf{M}(\mathbf{q})\ddot{\mathbf{q}} + \mathbf{C}(\mathbf{q}, \dot{\mathbf{q}})\dot{\mathbf{q}} + \mathbf{G}(\mathbf{q}) + \mathbf{d} \tag{14}$$

where $\mathbf{q}, \dot{\mathbf{q}}, \ddot{\mathbf{q}} \in \mathbb{R}^n$ are the output angle, angular velocity, and angular acceleration of the manipulator; $\mathbf{M}(\mathbf{q}) \in \mathbb{R}^{n\times n}$ is the symmetric positive definite inertia matrix; $\mathbf{C}(\mathbf{q}, \dot{\mathbf{q}}) \in \mathbb{R}^{n\times n}$ is the Coriolis and centripetal torque matrix; $\mathbf{G}(\mathbf{q}) \in \mathbb{R}^{n\times 1}$ is the gravity; $\mathbf{d} \in \mathbb{R}^{n\times 1}$ is the external disturbance; and $\boldsymbol{\tau} \in \mathbb{R}^n$ is the input control torque.

To simplify the controller design, define

$$\begin{cases} \mathbf{x}_1 = \mathbf{q} \\ \mathbf{x}_2 = \dot{\mathbf{q}} \\ \mathbf{y} = \mathbf{x}_1 \end{cases} \tag{15}$$

Then, the state space expression of SCARA can be designed as

$$\begin{cases} \dot{\mathbf{x}}_1 &= \mathbf{x}_2 \\ \dot{\mathbf{x}}_2 &= \mathbf{M}^{-1}(\mathbf{x}_1)(\boldsymbol{\tau} - \mathbf{C}(\mathbf{x}_1, \mathbf{x}_2)\mathbf{x}_2 - \mathbf{G}(\mathbf{x}_1) - \mathbf{d}) \\ \mathbf{y} &= \mathbf{x}_1 \end{cases} \tag{16}$$

The first dynamic surface is defined as

$$\mathbf{S}_1 = \mathbf{x}_1 - \mathbf{x}_{1d} \tag{17}$$

The second dynamic surface is defined as

$$\mathbf{S}_2 = \mathbf{x}_2 - \boldsymbol{\alpha}_1 \tag{18}$$

where $\mathbf{S}_1$ and $\mathbf{S}_2$ are the error vectors[31]; $\mathbf{x}_{1d}$ is the expectation track, which the goal is to make $\mathbf{x}_1$ track the desired input value $\mathbf{x}_{1d}$; and α_1 is the output of the low-pass filter $\bar{\mathbf{x}}_2$, which is defined as

$$\begin{cases} \bar{\mathbf{x}}_2 = -c_1\mathbf{S}_1 + \dot{\mathbf{x}}_{1d} \\ \bar{\mathbf{x}}_2 = u\dot{\boldsymbol{\alpha}}_1 + \boldsymbol{\alpha}_1 \\ \bar{\mathbf{x}}_2(0) = \boldsymbol{\alpha}_1(0) \end{cases} \tag{19}$$

where c_1 is a positive number greater than zero and u is the filter coefficient.

Then the filter error is defined as

$$\xi = \boldsymbol{\alpha}_1 - \bar{\mathbf{x}}_2 \tag{20}$$

The Lyapunov function is defined based on position tracking error, virtual control, and filter error

$$V_1 = \frac{1}{2}\mathbf{S}_1^{\mathrm{T}}\mathbf{S}_1 + \frac{1}{2}\mathbf{S}_2^{\mathrm{T}}\mathbf{M}\mathbf{S}_2 + \frac{1}{2}\xi^{\mathrm{T}}\xi \tag{21}$$

Then, taking a derivative of equation (21), the stability analysis is expressed as follows

$$\begin{aligned} \dot{V}_1 = {} & \mathbf{S}_1^{\mathrm{T}}\dot{\mathbf{S}}_1 + \mathbf{S}_2^{\mathrm{T}}\mathbf{M}\dot{\mathbf{S}}_2 + \frac{1}{2}\mathbf{S}_2^{\mathrm{T}}\dot{\mathbf{M}}\mathbf{S}_2 + \xi^{\mathrm{T}}\dot{\xi}, \\ \dot{V}_1 = {} & \mathbf{S}_1^{\mathrm{T}}(\dot{\mathbf{x}}_1 - \dot{\mathbf{x}}_{1d}) + \mathbf{S}_2^{\mathrm{T}}\mathbf{M}(\dot{\mathbf{x}}_2 - \dot{\boldsymbol{\alpha}}_1) + \mathbf{S}_2^{\mathrm{T}}\mathbf{C}\mathbf{S}_2 \\ & + \xi^{\mathrm{T}}(\dot{\boldsymbol{\alpha}}_1 - \dot{\bar{\mathbf{x}}}_2), \\ \dot{V}_1 = {} & \mathbf{S}_1^{\mathrm{T}}(\mathbf{x}_2 - \boldsymbol{\alpha}_1 + \boldsymbol{\alpha}_1 - \bar{\mathbf{x}}_2 - c_1\mathbf{S}_1) + \mathbf{S}_2^{\mathrm{T}}\mathbf{M}(\mathbf{M}^{-1}\boldsymbol{\tau} \\ & - \mathbf{M}^{-1}\mathbf{C}\mathbf{x}_2 - \mathbf{M}^{-1}\mathbf{G} - \mathbf{M}^{-1}\mathbf{d} - \dot{\boldsymbol{\alpha}}_1) + \mathbf{S}_2^{\mathrm{T}}\mathbf{C}\mathbf{S}_2 \\ & + \xi^{\mathrm{T}}\left(\frac{\bar{\mathbf{x}}_2 - \boldsymbol{\alpha}_1}{u} + c_1\dot{\mathbf{S}}_1 - \ddot{\mathbf{x}}_{1d}\right) \end{aligned}$$

The final form of $\dot{V}_1$ is shown in

$$\begin{aligned} \dot{V}_1 = {} & \mathbf{S}_1^{\mathrm{T}}(\mathbf{S}_2 + \xi - c_1\mathbf{S}_1) \\ & + \mathbf{S}_2^{\mathrm{T}}(\boldsymbol{\tau} - \mathbf{C}\mathbf{x}_2 - \mathbf{G} - \mathbf{d} + \mathbf{C}\mathbf{S}_2 - \mathbf{M}\dot{\alpha}_1) \\ & + \xi^{\mathrm{T}}\left(\frac{-\xi}{u} + c_1\dot{\mathbf{S}}_1 - \ddot{\mathbf{x}}_{1d}\right) \end{aligned} \tag{22}$$

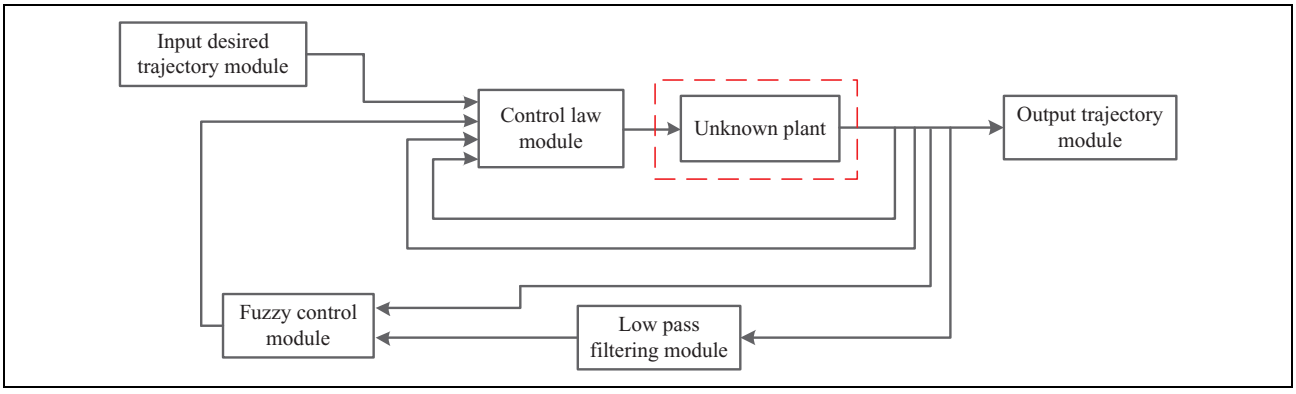

Figure 3. FADSC robot system. FADSC: fuzzy adaptive dynamic surface control.

According to the dynamic model structured in equation (10), the control law is designed as

$$\boldsymbol{\tau} = -c_2\mathbf{S}_2 - \mathbf{S}_1 - \boldsymbol{\xi} + \mathbf{G} + \mathbf{C}\boldsymbol{\alpha}_1 + \mathbf{M}\dot{\boldsymbol{\alpha}}_1 \tag{23}$$

Taking equation (23) into equation (22), then

$$\begin{aligned}\dot{V}_1 = &-c_1\mathbf{S}_1^{\mathrm{T}}\mathbf{S}_1 + \mathbf{S}_1^{\mathrm{T}}\boldsymbol{\xi} - c_2\mathbf{S}_2^{\mathrm{T}}\mathbf{S}_2 - \mathbf{S}_2^{\mathrm{T}}\boldsymbol{\xi} - \mathbf{S}_2^{\mathrm{T}}\mathbf{d} \\ &+ \boldsymbol{\xi}^{\mathrm{T}}\left(\frac{-\boldsymbol{\xi}}{u} + c_1(\mathbf{S}_2 + \boldsymbol{\xi} - c_1\mathbf{S}_1) - \ddot{\mathbf{x}}_{1d}\right)\end{aligned} \tag{24}$$

To simplify the calculation, let $c_1 = 1$, then

$$\dot{V}_1 = -\mathbf{S}_1^{\mathrm{T}}\mathbf{S}_1 - c_2\mathbf{S}_2^{\mathrm{T}}\mathbf{S}_2 - \mathbf{S}_2^{\mathrm{T}}\mathbf{d} - \left(\frac{1}{u} - 1\right)\boldsymbol{\xi}^{\mathrm{T}}\boldsymbol{\xi} - \boldsymbol{\xi}^{\mathrm{T}}\ddot{\mathbf{x}}_{1d} \tag{25}$$

where $\ddot{\mathbf{x}}_{1d}$ is the second derivative of the desired trajectory; according to Young's inequality, the following inequality holds

$$\begin{aligned}-\boldsymbol{\xi}^{\mathrm{T}}\ddot{\mathbf{x}}_{1d} &\le |\boldsymbol{\xi}^{\mathrm{T}}\ddot{\mathbf{x}}_{1d}| \\ &\le \frac{1}{2}\boldsymbol{\xi}^{\mathrm{T}}\boldsymbol{\xi} + \frac{1}{2}\ddot{\mathbf{x}}_{1d}^{\mathrm{T}}\ddot{\mathbf{x}}_{1d} \\ -\boldsymbol{\xi}^{\mathrm{T}}\ddot{\mathbf{x}}_{1d} &\le \frac{1}{2}\boldsymbol{\xi}^{\mathrm{T}}\boldsymbol{\xi} + \frac{1}{2}||\ddot{\mathbf{x}}_{1d}||^2\end{aligned} \tag{26}$$

Similarly to the analysis of ineq. (26), ineq. (27) holds

$$-\mathbf{S}_2^{\mathrm{T}}\mathbf{d} \le \frac{1}{2}\mathbf{S}_2^{\mathrm{T}}\mathbf{S}_2 + \frac{1}{2}||\mathbf{d}||^2 \tag{27}$$

Bring ineq. (26) and ineq. (27) into equation (25), then

$$\begin{aligned}\dot{V}_1 \le &-\mathbf{S}_1^{\mathrm{T}}\mathbf{S}_1 - \left(c_2 - \frac{1}{2}\right)\mathbf{S}_2^{\mathrm{T}}\mathbf{S}_2 - \left(\frac{1}{u} - \frac{3}{2}\right)\boldsymbol{\xi}^{\mathrm{T}}\boldsymbol{\xi} \\ &+ \frac{1}{2}||\ddot{\mathbf{x}}_{1d}||^2 + \frac{1}{2}||\mathbf{d}||^2\end{aligned} \tag{28}$$

Because $\ddot{\mathbf{x}}_{1d}$ and $\mathbf{d}$ are bounded, by selecting $u < \frac{2}{3}$ and appropriate value of c_2, it can be seen from equation (28) that $\dot{V}_1 < 0$; therefore the system is bounded and convergent for all signals in the closed-loop system.

The fuzzy adaptive DSC algorithm

As shown in equation (23), a traditional DSC is established on the model of SCARA. However, the traditional DSC algorithm needs specific parameters of the manipulator, such as the gravity $\mathbf{G}(\mathbf{q})$, the symmetric positive definite inertia matrix $\mathbf{M}(\mathbf{q})$, and the Coriolis and centripetal torque matrix $\mathbf{C}(\mathbf{q})$.

Due to the uncertainty of the dynamic model, the performance of DSC algorithm could be influenced. Therefore, based on the DSC algorithm, an approximate fuzzy algorithm is established to deal with the uncertainty, imprecision, and vagueness,[32] and a fuzzy adaptive DSC (FADSC) algorithm is proposed to ignore the model of the robot and improve the performance of the closed-loop system. The control structure of FADSC consists of six modules as shown in Figure 3. Comparing with the DSC control method in the third section, a fuzzy control module is proposed and the robot module which contains the robot model information is replaced by an unknown plant module.

Define $\mathbf{f}$ as the approximation part which contains the robot model information

$$\mathbf{f} = -\mathbf{C}\boldsymbol{\alpha}_1 - \mathbf{M}\dot{\boldsymbol{\alpha}}_1 - \mathbf{G} \tag{29}$$

Defining a fuzzy system named φ, the fuzzy rules are exhibited as

IF

x_1 is $\mu_{M_1^i}$ and x_2 is $\mu_{M_2^i}$ and $\ldots$ x_j is $\mu_{M_j^i}$ $j = 1, 2, \ldots, n$

THEN

$\mathbf{Y}$ is B^i, $i = 1, 2, \ldots, N$

where N is the number of total fuzzy rules, $\mathbf{x}$ is an input vector with the form of $\mathbf{x} = [x_1, x_2, \ldots, x_n]^{\mathrm{T}} \in \mathbb{R}^n$, $\mu_{M_j^i}$ is the membership function of the input variables $\mathbf{x} = [x_1, x_2, \ldots, x_n]^{\mathrm{T}} \in \mathbb{R}^n$, and B_i is the output fuzzy set of the ith fuzzy rule.

Within the author's cognition, the defuzzification methods in fuzzy system contain center of gravity defuzzification method, center average defuzzification method, and maximum defuzzification method. The center average defuzzification method used in this article is the most widely used and effective defuzzification method. Then, singleton fuzzifier and product inference[33] are used to establish the output of the fuzzy system

$$\mathbf{Y} = \frac{\sum_{i=1}^{N} \phi_i \prod_{j=1}^{n} \mu_{M_j^i}(x_j)}{\sum_{i=1}^{N} \prod_{j=1}^{n} \mu_{M_j^i}(x_j)} = \gamma^{\mathrm{T}}(\mathbf{x})\phi \tag{30}$$

where

$$\gamma = [\gamma_1(\mathbf{x}), \gamma_2(\mathbf{x}), \ldots, \gamma_N(\mathbf{x})]^{\mathrm{T}}; \phi = [\phi_1, \phi_2, ..., \phi_N]^{\mathrm{T}}$$

$$\gamma_i(\mathbf{x}) = \frac{\prod_{j=1}^{n} \mu_{M_j^i}(x_j)}{\sum_{i=1}^{N} \prod_{j=1}^{n} \mu_{M_j^i}(x_j)}$$

γ is the fuzzy weighting vector and ϕ is the parameter vector.

For the fuzzy approximation of $\mathbf{f}, f(1), f(2), f(3)$, and $f(4)$ are the elements of the vector $\mathbf{f}$, then the corresponding fuzzy system is designed to approximate $f(1)$, $f(2)$, $f(3)$, and $f(4)$. The fuzzy system is designed as[33]

$$\varphi_k(\mathbf{x}) = \frac{\sum_{i=1}^{N} \phi_{ki} \prod_{j=1}^{n} \mu_{M_j^i}(x_j)}{\sum_{i=1}^{N} \prod_{j=1}^{n} \mu_{M_j^i}(x_j)} = \gamma_k^{\mathrm{T}}(\mathbf{x})\phi_k \tag{31}$$

$$\varphi = \begin{bmatrix} \gamma_1^{\mathrm{T}} & \mathbf{0} & \mathbf{0} & \mathbf{0} \\ \mathbf{0} & \gamma_2^{\mathrm{T}} & \mathbf{0} & \mathbf{0} \\ \mathbf{0} & \mathbf{0} & \gamma_3^{\mathrm{T}} & \mathbf{0} \\ \mathbf{0} & \mathbf{0} & \mathbf{0} & \gamma_4^{\mathrm{T}} \end{bmatrix} \begin{bmatrix} \phi_1 \\ \phi_2 \\ \phi_3 \\ \phi_4 \end{bmatrix} = \gamma^{\mathrm{T}}(\mathbf{x})\phi \tag{32}$$

where φ is the output of the fuzzy system. According to equations (23) and (29), the FADSC control law is

$$\tau = -c_2\mathbf{S}_2 - \mathbf{S}_1 - \boldsymbol{\xi} - \boldsymbol{\varphi} \tag{33}$$

Defining the best approximation constant as ϕ^* and a compact set as $\Omega \in \mathbb{R}^n$, for the continuous fuzzy function $\mathbf{f}$, given any small constant $\varepsilon(\varepsilon > 0)$, there exists a fuzzy system which satisfies the following inequation

$$||\mathbf{f} - \boldsymbol{\varphi}^*|| \leq \varepsilon \tag{34}$$

The error $\tilde{\phi}$ between ϕ^* and ϕ is defined as

$$\tilde{\phi} = \phi^* - \phi \tag{35}$$

Then, the designed adaptive control law is defined as

$$\dot{\phi} = m\left(\mathbf{S}_2^{\mathrm{T}}\gamma^{\mathrm{T}}(x)\right)^{\mathrm{T}} - 2k\phi \tag{36}$$

The Lyapunov function is defined as

$$V = \frac{1}{2}\mathbf{S}_1^{\mathrm{T}}\mathbf{S}_1 + \frac{1}{2}\mathbf{S}_2^{\mathrm{T}}\mathbf{M}\mathbf{S}_2 + \frac{1}{2}\boldsymbol{\xi}^{\mathrm{T}}\boldsymbol{\xi} + \frac{1}{2m}\tilde{\phi}^{\mathrm{T}}\tilde{\phi} \tag{37}$$

For the convenience of calculation, let $c_1 = 1$, the stability analysis is as follows

$$\begin{aligned}
\dot{V} = & \quad \dot{V}_1 - \frac{1}{m}\tilde{\phi}^{\mathrm{T}}\dot{\phi} \\
\dot{V} = & \quad -\mathbf{S}_1^{\mathrm{T}}\mathbf{S}_1 - c_2\mathbf{S}_2^{\mathrm{T}}\mathbf{S}_2 - \left(\frac{1}{u} - 1\right)\boldsymbol{\xi}^{\mathrm{T}}\boldsymbol{\xi} \\
& + \mathbf{S}_2^{\mathrm{T}}(\mathbf{f} - \gamma^{\mathrm{T}}(\mathbf{x})\phi^*) + \mathbf{S}_2^{\mathrm{T}}(\gamma^{\mathrm{T}}(\mathbf{x})\phi^* - \gamma^{\mathrm{T}}(\mathbf{x})\phi) \\
& - \boldsymbol{\xi}^{\mathrm{T}}\ddot{\mathbf{x}}_{1d} - \mathbf{x}_2^{\mathrm{T}}\mathbf{d}] - \frac{1}{m}\tilde{\phi}^{\mathrm{T}}\dot{\phi} \\
\dot{V} \leq & \quad -\mathbf{S}_1^{\mathrm{T}}\mathbf{S}_1 - c_2\mathbf{S}_2^{\mathrm{T}}\mathbf{S}_2 - \left(\frac{1}{u} - 1\right)\xi^{\mathrm{T}}\xi + \frac{1}{2}||\mathbf{S}_2||^2 \\
& + \frac{1}{2}\varepsilon^2 + \frac{1}{2}||\mathbf{S}_2||^2 + \frac{1}{2}||\mathbf{d}||^2 + \frac{1}{2}||\xi||^2 + \frac{1}{2}||\ddot{\mathbf{x}}_{1d}||^2 \\
& + \tilde{\phi}^{\mathrm{T}}\left[(\mathbf{S}_2^{\mathrm{T}}\gamma^{\mathrm{T}}(\mathbf{x}))^{\mathrm{T}} - \frac{1}{m}(m(\mathbf{S}_2^{\mathrm{T}}\gamma^{\mathrm{T}}(\mathbf{x}))^{\mathrm{T}} - 2k\phi)\right] \\
\dot{V} \leq & \quad -\mathbf{S}_1^{\mathrm{T}}\mathbf{S}_1 - (c_2 - 1)\mathbf{S}_2^{\mathrm{T}}\mathbf{S}_2 - \left(\frac{1}{u} - \frac{3}{2}\right)\boldsymbol{\xi}^{\mathrm{T}}\boldsymbol{\xi} \\
& + \frac{1}{2}||\ddot{\mathbf{x}}_{1d}||^2 + \frac{1}{2}\varepsilon^2 + \frac{1}{2}\mathbf{d}^{\mathrm{T}}\mathbf{d} + \frac{k}{m}(2\phi^{*\mathrm{T}}\phi - 2\phi^{\mathrm{T}}\phi)
\end{aligned}$$

Therefore, the derivative of Lyapunov function $\dot{V}$ satisfies

$$\begin{aligned}
\dot{V} \leq & \quad -\mathbf{S}_1^{\mathrm{T}}\mathbf{S}_1 - (c_2 - 1)\mathbf{S}_2^{\mathrm{T}}\mathbf{S}_2 - \left(\frac{1}{u} - \frac{3}{2}\right)\boldsymbol{\xi}^{\mathrm{T}}\boldsymbol{\xi} \\
& + \frac{1}{2}||\ddot{\mathbf{x}}_{1d}||^2 + \frac{1}{2}\varepsilon^2 + \frac{1}{2}\mathbf{d}^{\mathrm{T}}\mathbf{d} + \frac{k}{m}(2\phi^{*\mathrm{T}}\phi - 2\phi^{\mathrm{T}}\phi)
\end{aligned} \tag{38}$$

It is obvious that $(\phi - \phi^*)^{\mathrm{T}}(\phi - \phi^*) \geq 0$, therefore $2\phi^{*\mathrm{T}}\phi - 2\phi^{\mathrm{T}}\phi \leq -\phi^{\mathrm{T}}\phi + \phi^{*\mathrm{T}}\phi^*$.

Substituting the above ineq. (38), the following inequation is obtained

$$\begin{aligned}
\dot{V} \leq & \quad -\mathbf{S}_1^{\mathrm{T}}\mathbf{S}_1 - (c_2 - 1)\mathbf{S}_2^{\mathrm{T}}\mathbf{S}_2 - \left(\frac{1}{u} - \frac{3}{2}\right)\boldsymbol{\xi}^{\mathrm{T}}\boldsymbol{\xi} \\
& + \frac{1}{2}||\ddot{\mathbf{x}}_{1d}||^2 + \frac{1}{2}\varepsilon^2 + \frac{1}{2}\mathbf{d}^{\mathrm{T}}\mathbf{d} \\
& + \frac{k}{m}(-\phi^{\mathrm{T}}\phi - \phi^{*\mathrm{T}}\phi^*) + \frac{2k}{m}\phi^{*\mathrm{T}}\phi^*
\end{aligned} \tag{39}$$

For $(\phi^* + \phi)^{\mathrm{T}}(\phi^* + \phi) \geq 0$, $-\phi^{*\mathrm{T}}\phi - \phi^{\mathrm{T}}\phi^* \leq \phi^{\mathrm{T}}\phi + \phi^{*\mathrm{T}}\phi^*$; combining equation (34), the following inequation is obtained

$$\begin{cases} \tilde{\phi}^{\mathrm{T}}\tilde{\phi} \leq 2\phi^{\mathrm{T}}\phi + 2\phi^{*\mathrm{T}}\phi^* \\ -\frac{1}{2}\tilde{\phi}^{\mathrm{T}}\tilde{\phi} \geq -\phi^{\mathrm{T}}\phi - \phi^{*\mathrm{T}}\phi^* \end{cases} \tag{40}$$

Using ineq. (40) to substitute ineq. (39), then we obtain

$$\begin{aligned} \dot{V} \leq & -\frac{2}{2}\mathbf{S}_1^{\mathrm{T}}\mathbf{S}_1 - (c_2 - 1)\frac{2}{2}\mathbf{S}_2^{\mathrm{T}}\mathbf{M}^{-1}\mathbf{M}\mathbf{S}_2 \\ & -\frac{2}{2}\left(\frac{1}{u} - \frac{3}{2}\right)\boldsymbol{\xi}^{\mathrm{T}}\boldsymbol{\xi} + \frac{1}{2}||\ddot{\mathbf{x}}_{1d}||^2 + \frac{1}{2}\varepsilon^2 \\ & +\frac{1}{2}\mathbf{d}^{\mathrm{T}}\mathbf{d} - \frac{k}{2m}\tilde{\phi}^{\mathrm{T}}\tilde{\phi} + \frac{2k}{m}\phi^{*\mathrm{T}}\phi^* \end{aligned} \tag{41}$$

Because $\mathbf{M}$ is a bounded symmetric positive definite matrix, there exists a positive number σ, which satisfies

$$\mathbf{M} \leq \sigma\mathbf{I} \tag{42}$$

Therefore, by simply transforming ineq. (42), ineq. (43) is obtained

$$-\mathbf{M}^{-1} \leq -\frac{1}{\sigma}\mathbf{I} \tag{43}$$

Substituting equation (41) by equation (43), then

$$\begin{aligned} \dot{V} \leq & -\frac{2}{2}\mathbf{S}_1^{\mathrm{T}}\mathbf{S}_1 - (c_2 - 1)\frac{2}{2\sigma}\mathbf{S}_2^{\mathrm{T}}\mathbf{M}\mathbf{S}_2 \\ & -\frac{2}{2}\left(\frac{1}{u} - \frac{3}{2}\right)\boldsymbol{\xi}^{\mathrm{T}}\boldsymbol{\xi} + \frac{1}{2}||\ddot{\mathbf{x}}_{1d}||^2 + \frac{1}{2}\varepsilon^2 \\ & +\frac{1}{2}\mathbf{d}^{\mathrm{T}}\mathbf{d} - \frac{k}{2m}\tilde{\phi}^{\mathrm{T}}\tilde{\phi} + \frac{2k}{m}\phi^{*\mathrm{T}}\phi^* \end{aligned} \tag{44}$$

Define a constant $c_0 = \min\{2, 2(c_2 - 1)\frac{1}{\sigma}, 2(\frac{1}{u} - \frac{3}{2}), k\}$, then use c_0 to substitute ineq. (44)

$$\begin{aligned} \dot{V} \leq & -\frac{c_0}{2}\left(\mathbf{S}_1^{\mathrm{T}}\mathbf{S}_1 + \mathbf{S}_2^{\mathrm{T}}\mathbf{M}\mathbf{S}_2 + \boldsymbol{\xi}^{\mathrm{T}}\boldsymbol{\xi} + \frac{1}{m}\tilde{\phi}^{\mathrm{T}}\tilde{\phi}\right) \\ & + \frac{2k}{m}\phi^{*\mathrm{T}}\phi^* + \frac{1}{2}\varepsilon^2 + \frac{1}{2}\mathbf{d}^{\mathrm{T}}\mathbf{d} + \frac{1}{2}||\ddot{\mathbf{x}}_{1d}||^2 \\ \dot{V} \leq & -c_0 V + \frac{2k}{m}\phi^{*\mathrm{T}}\phi^* + \frac{1}{2}\varepsilon^2 + \frac{1}{2}\mathbf{d}^{\mathrm{T}}\mathbf{d} + \frac{1}{2}||\ddot{\mathbf{x}}_{1d}||^2 \end{aligned}$$

There must be $D > 0$ because of the bounded external interference, which must satisfy $\mathbf{d}^{\mathrm{T}}\mathbf{d} \leq D$. $\ddot{\mathbf{x}}_{1d}$ is the second derivative of the expected trajectory, and also the bounded function. There must be $E > 0$. It must satisfy the formula $||\ddot{\mathbf{x}}_{1d}||^2 \leq E$. Therefore

$$\dot{V} \leq -c_0 V + \frac{2k}{m}\phi^{*\mathrm{T}}\phi^* + \frac{1}{2}\varepsilon^2 + \frac{D}{2} + \frac{E}{2}$$

Let $c_V = \frac{2k}{m}\phi^{*\mathrm{T}}\phi^* + \frac{1}{2}\varepsilon^2 + \frac{D}{2} + \frac{E}{2}$, therefore

$$\dot{V} \leq -c_0 V + c_V \tag{45}$$

Define the compact set $\Omega_0 = \left\{x | V(x) \leq V(0) + \frac{c_V}{c_0}\right\}$, $\{\mathbf{S}_1, \mathbf{S}_2, \boldsymbol{\xi}, \tilde{\phi}\} \in \Omega_0$. Solve ineq. (45)

$$\begin{aligned} V(t) &\leq V(0)\exp(-c_0 t) + \frac{c_V}{c_0}[1 - \exp(-c_0 t)] \\ &\leq V(0) + \frac{c_V}{c_0}, \forall t \geq 0 \end{aligned} \tag{46}$$

where $V(0)$ is the initial value of V.

From ineq. (46), it can be concluded that V is bounded, and therefore all signals of the closed-loop system are bounded. From the above derivation, we can see that the FADSC algorithm does not need the exact parameters of the SCARA manipulator. Thus the system is robust under modeling uncertainty.

Simulation results and analysis

We define the following parameters of mechanical structure with the SCARA robot, Athena's AH-4520-054 S[34] as reference

$$m_1 = 10\mathrm{kg}, m_2 = 5\mathrm{kg}, m_3 = m_4 = 3\mathrm{kg}$$
$$l_1 = 200\mathrm{mm}, l_2 = 250\mathrm{mm}, r = 30\mathrm{mm}$$

Two kinds of signals are chosen as input position instructions, which are mixed sine signal and triangle signal. The tracking abilities of DSC and FADSC are investigated in this section. The input desired trajectories are in the following forms:

The desired trajectory 1

$$q_{d_1} = q_{d_2} = q_{d_4} = d_3 = 0.2\sin(5t) + 0.2\sin(3t) + 0.2\sin(t)$$

The desired trajectory 2

$$q_{d_1} = q_{d_2} = q_{d_4} = d_3 = \begin{cases} k(x - 2.5m) & m = 0, \pm 1, \ldots \\ -k(x - 2.5n) & n = \pm 1, \pm 2, \ldots \end{cases}$$

For the third vertical joint, as a result of the influence of gravity and velocity mutation, k is chosen as 0.16, for all the other three joints $k = 0.4$.

The initial state of the system is zero. The control period of the system is chosen as 1ms. The external disturbance on the torque is in the form of

$$\begin{aligned} \mathbf{d} = & f_c \mathrm{sgn}(\dot{q}_i)\left(\left[1 - \exp\left(\frac{-\dot{q}_i^2}{s^2}\right)\right]\right) \\ & + f_s \mathrm{sgn}(\dot{q}_i)\left(\left[\exp\left(\frac{-\dot{q}_i^2}{s^2}\right)\right]\right) + f_v\dot{q}_i \end{aligned}$$

where $f_c = [3.1; 2.7; 0.75; 16]$ is the Coulomb coefficient,

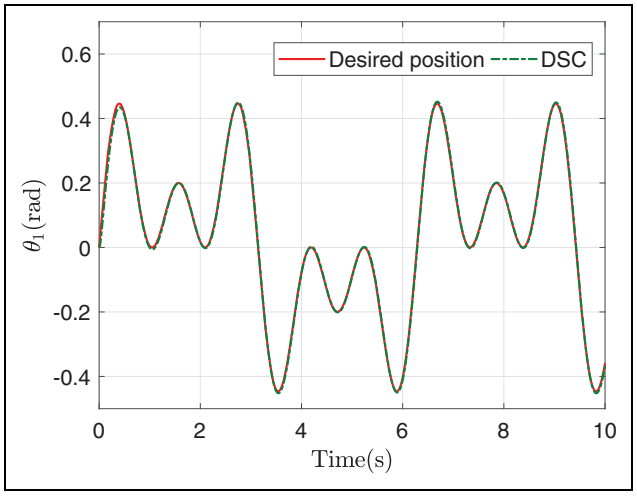

Figure 4. Input mixed sine signal and position tracking results without disturbance: taking joint 1 for example. DSC: dynamic surface control.

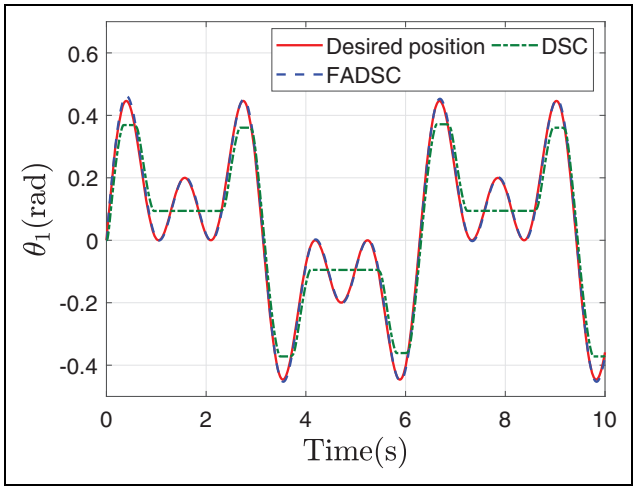

Figure 5. Input mixed sine signal and position tracking results with disturbance: taking joint 1 for example. DSC: dynamic surface control; FADSC: fuzzy adaptive dynamic surface control.

$f_s = [19; 19; 9.5; 100]$ is the static coefficient, $f_v = [0.9; 0.9; 0.6; 6]$ is the viscous coefficient, and $s = [0.39; 0.39; 0.15; 0.39]$ is the Stribeck parameter.

The disturbance on the robot model is random, while it has an upper limit form of

$$\Delta\mathbf{M} = 0.2\sin(2t)\mathbf{M}, \Delta\mathbf{C} = 0.1\sin(2t)\mathbf{C}$$
$$\Delta\mathbf{G} = 0.05\sin(2t)\mathbf{G}$$

The controller parameters c_2 and k are 50 and 15, respectively; the filter coefficient u is 0.01; and the adaptive control law coefficient m is 200. In the simulation study, three fuzzy sets are defined over interval $[-1.25, 1.25]$ for all states, and by choosing partitioning points as -1.25, 0, and 1.25, their fuzzy membership functions are given as follows

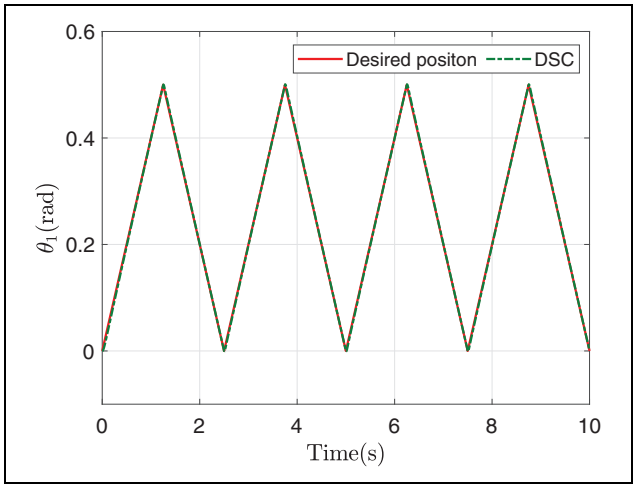

Figure 6. Input triangle signal and position tracking results without disturbance: taking joint 1 for example. DSC: dynamic surface control.

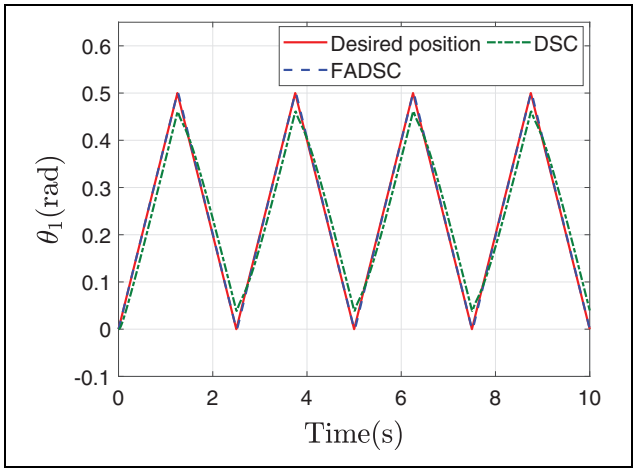

Figure 7. Input triangle signal and position tracking results with disturbance: taking joint 1 for example. DSC: dynamic surface control; FADSC: fuzzy adaptive dynamic surface control.

$$\mu_{F_i^1} = \exp\left[-0.5\left(\frac{x_i + 1.25}{0.6}\right)^2\right]$$
$$\mu_{F_i^2} = \exp\left[-0.5\left(\frac{x_i}{0.6}\right)^2\right]$$
$$\mu_{F_i^3} = \exp\left[-0.5\left(\frac{x_i - 1.25}{0.6}\right)^2\right]$$

where $i = 1, 2, 3, 4$.

According to the two controllers designed in equations (23) and (33), we get the simulation results with trajectories 1 and 2, respectively. Figures 4 to 7 show the simulation results of the tracking process under friction disturbance and model uncertainty. To verify the effectiveness of the

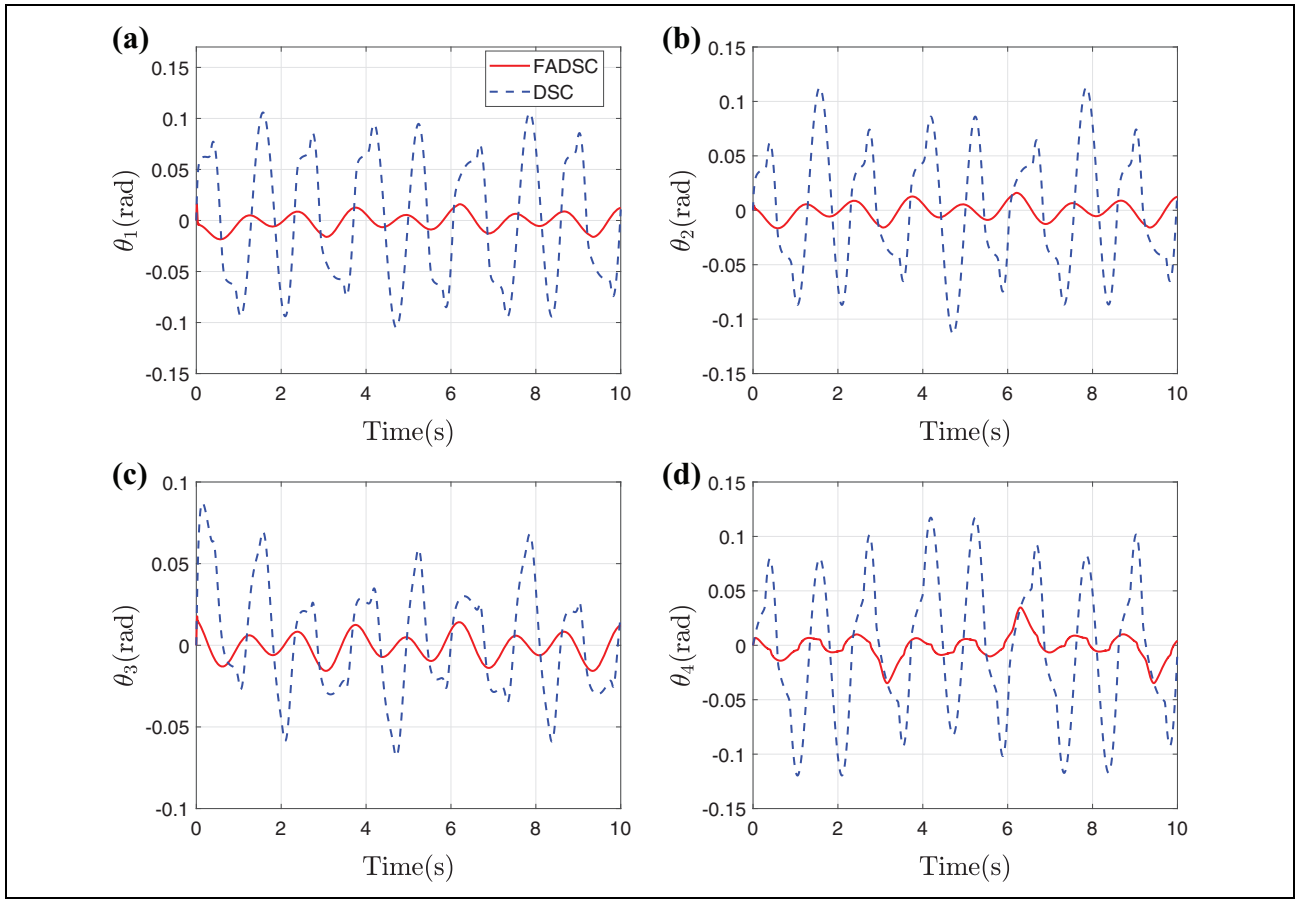

Figure 8. Position tracking error comparison of desired trajectory 1: (a) joint 1, (b) joint 2, (c) joint 3, and (d) joint 4. DSC: dynamic surface control; FADSC: fuzzy adaptive dynamic surface control.

proposed algorithm, two experiments were conducted, mixed sine signals and triangle signal are selected as instruction position. From the comparison between Figures 4 and 5, and the comparison between Figures 6 and 7, it can be seen that the traditional DSC algorithm is capable of tracking desired sine input location curve almost successfully; however, the external disturbance causes negative influence on the phase position. Figure 5 gives the comparison of position tracking results under the mixed sine signal with disturbance. It is clear that the traditional DSC has poor performance when it tracks the peak value of sine signal especially. In addition, Figure 7 explores the position following ability with input triangle signal, from which we can see that the traditional DSC does not respond to the instructions fast enough.

Figures 8 and 9 give details of error comparison when DSC and FADSC tracking the desired trajectories 1 and 2, respectively, all of the four position tracking errors with respect to the corresponding four joints of the SCARA are investigated. It can be considered that FADSC has better tracking accuracy and faster response compared to the traditional DSC.

Tables 2 and 3 show the position tracking results of the numerical analysis of traditional DSC and FADSC. To analyze the simulation results, we adopt a set of simple parameters to quantify the performance more clearly. The maximum absolute peaking error (MAPE) and the integral of absolute error (IAE) were calculated and shown in Tables 2 and 3. From the simulation results, the FADSC also shows a better performance. Taking joint 1 for example, when tracking the desired trajectory 1, FADSC decreased 91.61% of IAE and 83.33% of MAPE for the position tracking; when tracking the desired trajectory 2, FADSC decreased 88.18% of IAE and 90% of MAPE for the position tracking. Furthermore, for all the four joints, the traditional DSC is fluctuating on position error in whole 10 s, while proposed algorithm reached its stable state faster with smaller tracking errors.

Conclusion

In conclusion, this article applies both traditional DSC and proposed FADSC algorithms on the SCARA manipulator.

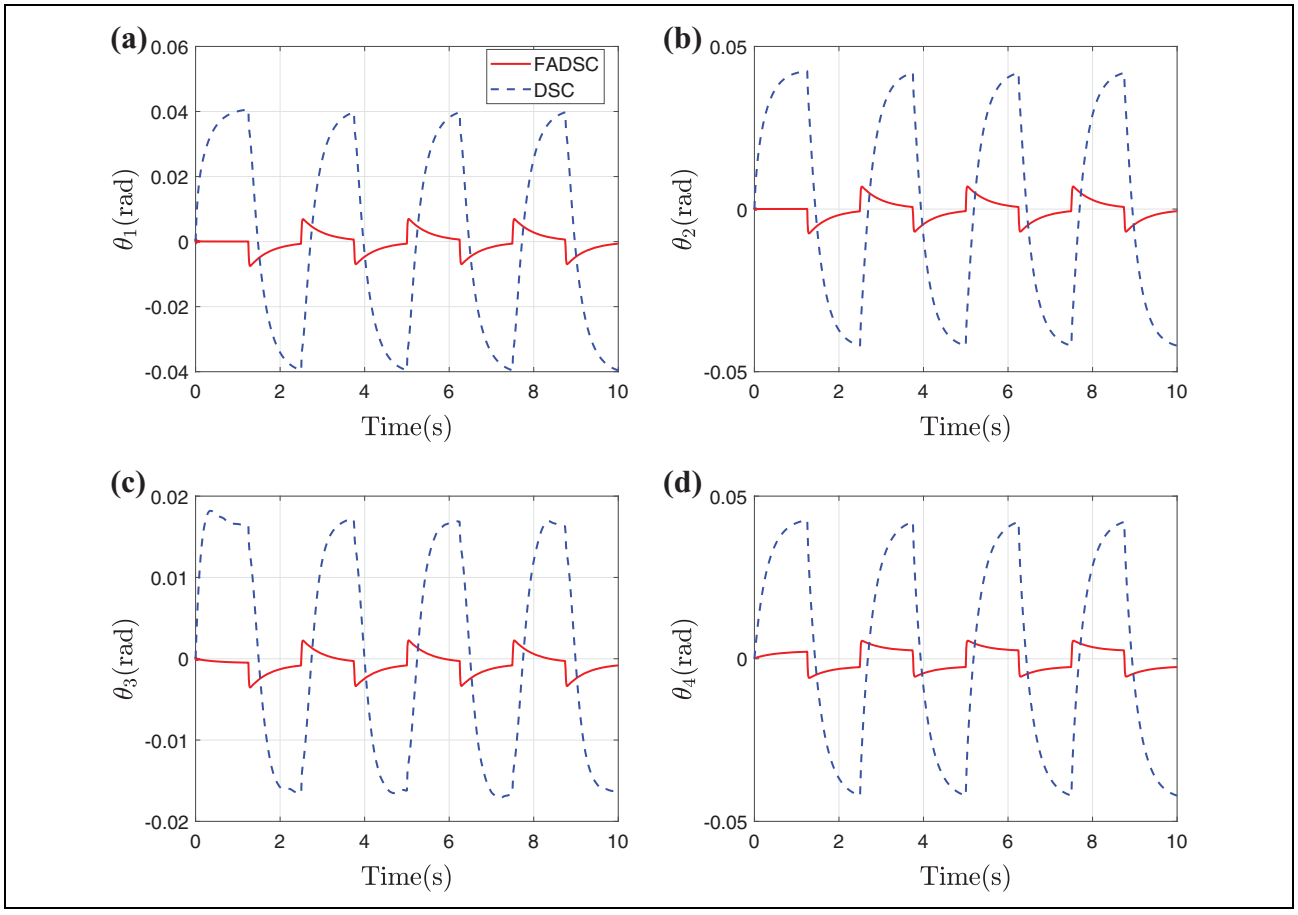

Figure 9. Position tracking error comparison of desired trajectory 2: (a) joint 1, (b) joint 2, (c) joint 3, and (d) joint 4. DSC: dynamic surface control; FADSC: fuzzy adaptive dynamic surface control.

Table 2. Position tracking error analysis of trajectory 1.

	Traditional DSC		FADSC	
Method	MAPE	IAE	MAPE	IAE
Joint 1	0.105	0.0286	0.0175	0.0024
Joint 2	0.11	0.0306	0.0175	0.0024
Joint 3	0.08	0.0129	0.0175	0.0011
Joint 4	0.115	0.0299	0.0375	0.0032

DSC: dynamic surface control; FADSC: fuzzy adaptive dynamic surface control; MAPE: maximum absolute peaking error; IAE: integral of absolute error.

Table 3. Position tracking error analysis of trajectory 2.

	Traditional DSC		FADSC	
Method	MAPE	IAE	MAPE	IAE
Joint 1	0.04	0.0584	0.004	0.0069
Joint 2	0.04	0.0491	0.005	0.0067
Joint 3	0.0085	0.0293	0.002	0.0066
Joint 4	0.04	0.0558	0.005	0.0088

DSC: dynamic surface control; FADSC: fuzzy adaptive dynamic surface control; MAPE: maximum absolute peaking error; IAE: integral of absolute error.

The simulation results prove the effectiveness of the new algorithm, which has a higher performance on position tracking tasks. Besides, comparing with the traditional DSC algorithm, FADSC do not need accurate parameters of the manipulator. The external disturbances and modeling error have an obvious influence on the closed-loop system of the controller designed by the traditional DSC algorithm, but have almost no impact on the proposed closed-loop system. Simulation results show the effectiveness of the proposed model-free controller with high-speed tracking capability and high stability, which can be extended to multi-joint manipulators for the applications of robot arm with uncertain parameters.

Declaration of conflicting interests

The author(s) declared no potential conflicts of interest with respect to the research, authorship, and/or publication of this article.

Funding

The author(s) disclosed receipt of the following financial support for the research, authorship, and/or publication of this article: This research was supported by the National Natural Science Foundation of China (61973099), Fundamental Research Funds for the Central University (HIT.NSRIF.2017025, HIT.NSRIF.2019052),

the China Postdoctoral Science Foundation (2017M621259, 2016M591532), and the Heilongjiang Postdoctoral Fund (LBH-Z16062).

References

1. Yang J and Kim J. Sliding mode control for trajectory tracking of nonholonomic wheeled mobile robots. *IEEE Trans Robot Autom* 1999; 15(3): 578–587.
2. Xia Y, Xie W, and Ma J. Research on trajectory tracking control of manipulator based on modified terminal sliding mode with double power reaching law. *Int J Adv Robot Syst* 2019; 16(3).
3. Qin H, Wu Z, Sun Y, et al. Prescribed performance adaptive fault-tolerant trajectory tracking control for an ocean bottom flying node. *Int J Adv Robot Syst* 2019; 16(3).
4. Abad EC, Alonso JM, Garcia MJG, et al. Methodology for the navigation optimization of a terrain-adaptive unmanned ground vehicle. *Int J Adv Robot Syst* 2018; 15(1).
5. Coelho P and Nunes U. Path-following control of mobile robots in presence of uncertainties. *IEEE Trans Robot* 2005; 21(2): 252–261.
6. Matveev AS, Wang C, and Savkin AV. Real-time navigation of mobile robots in problems of border patrolling and avoiding collisions with moving and deforming obstacles. *Robot Auton Syst* 2012; 60(6): 769–788.
7. Makino H. Development of the SCARA. *J Robot Mechatron* 2014; 26(1): 5–8.
8. Visioli A and Legnani G. On the trajectory tracking control of industrial SCARA robot manipulators. *IEEE Trans Ind Electron* 2002; 49(1): 224–232.
9. Hsu H, Chu L, Wang Z, et al. Position control and novel application of SCARA robot with vision system. *Adv Technol Innovat* 2017; 2(2): 40–45.
10. Swaroop D, Gerdes J, Yip PP, et al. Dynamic surface control of nonlinear systems. In: *Proceedings of the 1997 American control conference*, Vol. 5, Albuquerque, NM, USA, 6 June 1997, pp. 3028–3034. IEEE.
11. Swaroop D, Hedrick JK, Yip PP, et al. Dynamic surface control for a class of nonlinear systems. *IEEE Trans Autom Control* 2000; 45(10): 1893–1899.
12. Wang D and Huang J. Neural network based adaptive dynamic surface control for nonlinear systems in strict-feedback form. In: *Proceedings of the 40th IEEE conference on decision and control*, Vol. 4, Orlando, FL, USA, 4–7 December 2001, pp. 3524–3529. IEEE.
13. Wang D and Huang J. Neural network-based adaptive dynamic surface control for a class of uncertain nonlinear systems in strict-feedback form. *IEEE Trans Neural Netw* 2005; 16(1): 195–202.
14. Yoo SJ, Park JB, and Choi YH. Adaptive dynamic surface control for stabilization of parametric strict-feedback nonlinear systems with unknown time delays. *IEEE Trans Autom Control* 2007; 52(12): 2360–2365.
15. Zhang TP and Ge SS. Adaptive dynamic surface control of nonlinear systems with unknown dead zone in pure feedback form. *Automatica* 2008; 44(7): 1895–1903.
16. Pan H, Jing X, Sun W, et al. A bioinspired dynamics-based adaptive tracking control for nonlinear suspension systems. *IEEE Trans Control Syst Technol* 2018; 26(3): 903–914.
17. Soltanpour MR, Khooban MH, and Soltani M. Robust fuzzy sliding mode control for tracking the robot manipulator in joint space and in presence of uncertainties. *Robotica* 2013; 32(3): 433–446.
18. Long C, Hou ZG, and Min T. Adaptive neural network tracking control for manipulators with uncertain kinematics, dynamics and actuator model. *Automatica* 2009; 45(10): 2312–2318.
19. Chen CS. Dynamic structure neural-fuzzy networks for robust adaptive control of robot manipulators. *IEEE Trans Ind Electron* 2008; 55(9): 3402–3414.
20. Tong SC, Li YM, Feng G, et al. Observer-based adaptive fuzzy backstepping dynamic surface control for a class of MIMO nonlinear systems. *IEEE Trans Syst Man Cybern B* 2011; 41(4): 1124–1135.
21. Lee CH and Chung BR. Adaptive backstepping controller design for nonlinear uncertain systems using fuzzy neural systems. *Int J Syst Sci* 2012; 43(10): 1855–1869.
22. Pan H, Sun W, Gao H, et al. Disturbance observer-based adaptive tracking control with actuator saturation and its application. *IEEE Trans Autom Sci Eng* 2016; 13(2): 868–875.
23. Song B and Hedrick JK. *Dynamic surface control of uncertain nonlinear systems: an LMI approach*. Berlin: Springer Science & Business Media, 2011.
24. Wen S, Yu H, Zhang B, et al. Fuzzy identification and delay compensation based on the force/position control scheme of the 5-dof redundantly actuated parallel robot. *Int J Fuzzy Syst* 2017; 19(1): 124–140.
25. Makino H and Furuya N. Selective compliance assembly robot arm. In: *Proceedings of the 1st international conference on assembly automation*, Brighton, UK, 25–27 March 1980, pp. 77–86. IFS.
26. Urrea C and Kern J. Modeling, simulation and control of a redundant SCARA-type manipulator robot. *Int J Adv Robot Syst* 2012; 9(2): 58.
27. Padhy SK. On the dynamics of SCARA robot. *Robot Auton Syst* 1992; 10(1): 71–78.
28. Cai Z. *Robotics*. Beijing: Tsinghua University Press, 2000.
29. Dawson DM, Abdallah CT, and Lewis FL. *Robot manipulator control: theory and practice*. Boca Raton: CRC Press, 2003.
30. De Wit CC, Siciliano B, and Bastin G. *Theory of robot control*. Berlin: Springer Science & Business Media, 2012.
31. Liu J. *Sliding mode variable structure control MATLAB simulation*. Beijing: Tsinghua University Publish House, 2005.
32. Singh J, Prasad M, Prasad OK, et al. A novel fuzzy logic model for pseudo-relevance feedback-based query expansion. *Int J Fuzzy Syst* 2016; 18(6): 980–989.
33. Wang LX. *Theory of robot control*. New Jersey: Englewood Cliffs, 1994.
34. Technology Q. Athena's AH-4520-054s.